Journal of Coupled Systems and Multiscale Dynamics

doi:10.1166/jcsmd.2018.1172
J. Coupled Syst. Multiscale Dyn.
Vol. 6(4)/2330-152X/2018/310/007

Research Article

Electrical percolation in conductive granular media

Chongpu Zhai[1] and Yixiang Gan[2,*]

[1]*Hopkins Extreme Materials Institute, The Johns Hopkins University, Baltimore, MD 21218, United States*
[2]*School of Civil Engineering, The University of Sydney, NSW 2006, Australia*

(Received: 30 November 2018. Accepted: 26 December 2018)

ABSTRACT

In this study, electrical responses of conductive granular mixtures over a wide frequency range were investigated by focusing on the universal power-law scaling. The studied granular packings with various proportion of conductive grains were considered as resistor-capacitor networks based on contact fabrics and interfacial properties. With prescribed contact networks constructed from the discrete element method, we employed both percolation theories and circuit simulation to compute electrical responses, both of which well predict the span of power-law regimes obtained in experimental observations. This study reveals the role of percolation in controlling electrical responses of conductive granular materials and provide insight into testing techniques for granular energy materials and systems.

Keywords: RC Network, Contact Mechanics, Granular Materials, Electrical Transport, Universal Scaling.
Section: Mathematical, Physical & Engineering Sciences

1. INTRODUCTION

As one of intrinsic electrical properties, the 'universal dielectric responses' (UDR) characterised by power law scaling over a certain range of frequencies have been observed in different types of materials, such as metal nanoparticles,[1,2] random conductor-insulator mixtures,[3,4] disordered ceramics,[5,6] ion/electron-conducting glasses[6–8] and amorphous semiconductors.[7,9] This frequency-dependent behaviour is of significance in diverse applications including material characterization,[5,7] battery optimisation,[10] and electronic sensors.[11] For typical conductive granular materials,[12] the alternating current (AC) responses over a wide frequency range covering the UDR regime, exhibit at low and high frequencies, respectively, a resistive plateau and a state of nearly constant loss (NCL).[13–15] With proper normalization procedure described in Ref. [12], the AC responses obtained under various mechanical compression[12] were found to follow a single master curve. The electrical responses in granular materials have been investigated by effective-medium approximations (EMA),[13,18–20] 2D/3D lattice networks,[3,14,15,17,21,22] discrete element method modeling.[12,20,23] These approaches usually involve imposed assumptions of topological structures and transport mechanisms at the microscale.[12,13,24]

In the development of lithium-ion battery electrodes that can be meaningfully considered as granular materials,[19,20] electrochemical impedance spectroscopy (EIS) has been widely applied to monitor battery performance, predict the likelihood of failure and optimise battery design.[25,26] Specifically, the electrical responses of a non-destructive perturbating signal offer a wealth of information about the battery system such as, the reaction mechanisms, state of charge, kinetics at each electrode, passivating film behaviour, and possible electrode corrosion.[27] For lithium-ion batteries, the UDR together with the resistive plateau and NCL were typically observed in Bode plots[28,29] of EIS measurements, further featured by a transition from diffusional impedance to bulk impedance. This AC response is similar to that of conductive granular materials.[12,17] The EIS data are

*Author to whom correspondence should be addressed.
Email: yixiang.gan@sydney.edu.au

commonly analysed by fitting to a standard equivalent electrical circuit model which gives the best match to the measured data. Based on the physical characteristics and processes involved in the electrochemical cell, these models are partially or completely empirically chosen, consisting basic electrical elements, i.e., resistors, capacitors and inductors.[25, 30–34] For instance, the Randels cell model[32] includes a solution resistance and a double-layer capacitor in parallel with a charge-transfer resistance. However, these elements were phenomenologically implemented and usually lose the direct connection to microstructures and states of electrodes. The real energy systems can be considered as a large number of circuit elements with various of connection patterns exhibiting much more complex behaviour than that of simple equivalent circuits. Though nonlinear least squares procedures[28, 29, 35] have been adopted in simplified models with adjusted circuit parameters, in order to minimise the error obtained from numerical models, the physical origins of the dispersion between the experimental and numerical models remain unclear.

In this study, we employed both numerical and analytical approaches to elucidate the electrical transport of conductive granular materials, highlighting the role of percolation behaviour in dominating AC responses. The obtained numerical and analytical results were validated with measured AC spectra of conductive granular mixtures by focusing on the span of power-law scaling segments. Numerically, we simulated the AC responses of resistor-capacitor (RC) networks established from prescribed packing structures of various types and sizes. The onset and termination of power-law segment are respectively defined between the peaks found in spectra of imaginary impedance and electrical impedance module. Analytically, at low and high frequencies, we computed for different types of RC networks, respectively, the percolation-determined conductivity and permittivity. These values together with the universal centre[17] essentially determine the power-law segments. This study reveals fundamental drives shaping the AC responses for various conductive granular mixtures and sheds light upon testing techniques for characterising granular energy materials.

2. THEORETICAL BACKGROUND

2.1. Percolation Probability

Typical Bode plots for lithium-ion battery electrodes demonstrate a resistive plateau at low frequencies and NCL state at high frequencies.[28, 29] More generally, AC spectra for RC network can demonstrate different transition modes from low to high frequencies via a universal power law segment, including plateau-to-NCL, plateau-to-plateau, NCL-to-NCL, or NCL-to-plateau, primarily controlled by percolative conduction at both low and high frequencies. According to percolation theory, the effective electrical conductivity of a material is essentially determined by the percolation probability which represents the likelihood that particles are clustered in ways that form connected conduction pathways. For the calculation of the percolation probability, P, of a sphere mixture of M phases including conductive phase m and other non-conductive phases, an empirical formula has been put forward;[18, 36]

$$P = \left(1 - \left(\frac{3.764 - Z_{m,m}}{2}\right)^{2.5}\right)^{0.4} \tag{1}$$

where $Z_{m,m}$ is the average number of contacting particles of species m has to particles of the same species. The value of $Z_{m,m}$ is proportional to the surface-area fraction, δ_m, which is of all m particles, and the overall mean coordiantion number Z_0 ($Z_0 \approx 6.2$ for mono-sised random sphere pakcing). The coordination number $Z_{m,m}$ can be derived by

$$Z_{m,m} = Z_0 \delta_m = Z_0 \frac{P_m / r_m}{\sum_i^M P_i / r_i} \tag{2}$$

where r is the radius of the spheres. The surface-area fraction, δ_m, is defined in terms of the volume fractions P_m of the m particles:

$$\delta_m = \frac{P_m / r_m}{\sum_i^M \varphi_i / r_i}, \quad \varphi_k = \frac{n_m r_m^3}{\sum_i^M n_i r_i^3} \tag{3}$$

Noted that, at the contact level, a m-to-m contact may exhbit various frequency-dependent electrical conduction, depending on the interfacial conditions.

2.2. Electrical Contact

Each individual m-to-m contact can be considered as a resistor (R), a capacitor (C), or a resistor and a capacitor in parallel ($R//C$), depending on the interparticle force and interfacial properties, establishing a RC network throughout the granular packing.[12, 16, 37, 38] Specifically, adjacent particles can be treated initially as a capacitor, i.e., C. The interaction between two contacting particles under increasing compression will evolve from a capacitor, C, (due to the existing oxide layer and surface roughness) to an effective resistor in parallel with an effective capacitor, i.e., $R//C$, and eventually to a resistor, R, even a inductor.[12, 16, 37, 38] The interface tends to exhibit multiscale geometries governing interfacial electromechanical phenomena, and more details can be found in literature.[39–41] Different types of RC elements should be meaningfully selected for conductive granular mixture for various testing conditions. In this paper, $Z^*_{m,m\_R} = P_{Ri} Z_{m,m}$ describes the number of resistive contacts for low frequencies and $Z^*_{m,m\_C} = P_{Ci} Z_{m,m}$ indicates the number of contacts demonstrating capacitive properties at high frequencies. The probabilities of a contact being resistive and capacitive are indicated by P_{Ri} and P_{Ci}, respectively.

We show, in Figure 1, the probability of conductive granular mixture exhibiting the AC response with a transition from resistive plateau to NCL as frequency increases,

typical in EIS for lithium-ion battery electrodes.[28, 29] Here we considered a mono-sized granular mixture containing conductive grains (m) and non-conductive grains (n). For varying volume fraction of m, P_m, and varying resistor proportion, P_R (calculated based on P_{Ri}, P_{Ci} and RC network type, as is detailed in Ref. [12]), three types of RC networks were considered: (a) networks containing R and C elements ($R-C$), (b) networks built with C and $R//C$ elements ($C-R//C$), and (c) networks with R and $R//C$ elements ($R-R//C$). The probability of showing a transition from resistive plateau to NCL in AC responses was calculated by multiplying the resistive percolation probability at low frequency and the capacitive percolation probability at high frequency.

2.3. Resistive and Capacitive Percolation

The span of the observed emergent power-law segment is essential in determining the whole AC response. The exponent of the emergent power-law scaling is directly related to capacitor proportion, P_C in the established RC network, according to the mixing rule.[13–15, 22] For a given RC network, the emergent power-law scaling of varying P_C coincide at a universal intersection centre[17] at the frequency, f_I, where resistors and capacitors contribute equally to the overall conduction i.e., $1/R = 2\pi f_I C$. Further with conduction information at low and high frequencies, the whole AC spectrum can be well described. Percolation theory can be generally applied to calculate the effective conductivity for a mixture of conductive components having a certain conductivity of σ_R and permittivity of $\varepsilon_R \to \infty$, and dielectric components with a finite permittivity, ε_C, and conductivity, $\sigma_C = 0$, corresponding to the resistive and capacitive sites/bonds, respectively. Scenarios at low-frequency region ($\omega \to 0$) and high-frequency region ($\omega \to \infty$) can be represented by resistor-capacitor mixture and resistor-superconductor (capacitor) mixture,[42, 43] respectively. For a given sites/bonds network structure with varying resistor proportion P_R the effective conductivity at low frequency, σ_l^{eff}, and the permittivity at high frequencies, $\varepsilon_h^{\text{eff}}$, can be respectively calculated by

$$\sigma_l^{\text{eff}} = K_l \sigma_R (P_R - P_S)^t, \quad \varepsilon_h^{\text{eff}} = K_h \varepsilon_C (P_S - P_R)^{-s} \tag{4}$$

where $t = 1.9$ and $s = 0.73$ are constants depending on dimensionality of the network structure[42] and P_S is the percolation threshold, which can be computed using Monte Carlo method for a given structure.[42] For a structure with determined P_S, the values of K_l and K_h can be calculated, respectively, by assuming $P_R = 1$ and $P_R = 0$, with σ_l^{eff} and $\varepsilon_h^{\text{eff}}$ being σ_R and ε_C, respectively.[36, 44] Particularly, for a simple R-C network with all R and C elements having identical resistance and capacitance, the effective σ_R and ε_C can be calculated with $\sigma_R = RL/A$ and $\varepsilon_C = CA/L$, by considering network dimensions, i.e., cross-section, A, and length, L. Meanwhile, impedance terms, Z_l^{eff} and Z_h^{eff}, describing the resistive plateau and NCL can be obtained, respectively, from the reciprocals of σ_l^{eff} and $\omega\varepsilon_h^{\text{eff}}$, where ω is the frequency. For a given RC network with a certain proportion of capacitor, the universal centre[17] together with Z_l^{eff} and Z_h^{eff} can well shape the AC spectrum after determining the power-law segment, resistive plateau and NCL. Here, the span of two intersection points between the three segments defines the length of the power-law segment

3. NUMERICAL SIMULATION

To explore the origins of the frequency-dependent electrical transport of conductive granular mixture, we incorporated the electrical interaction between spheres into prescribed random packing structures using the discrete element method.[45] The obtained packing is sandwiched between two conductive rigid flats, one of which is grounded and the other is raised to a potential $V(\omega)$. The impedance can be obtained by solving the complex linear equations established by applying the Kirchhoff's current law to each particle, denoting a node of the network.[17] With this numerical strategy, we calculated the AC responses of RC network with various geometries. Figure 2 shows the dependence of normalised impedance

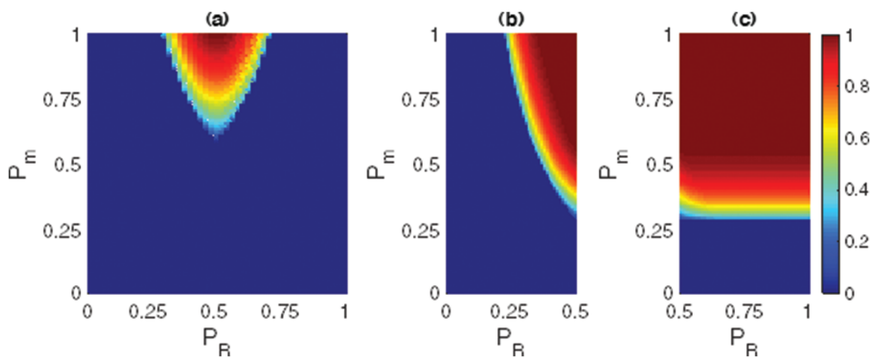

Fig. 1. The probability map of an AC response showing a resistive plateau at low frequencies and NCL state at high frequencies for various RC networks including (a) $R-C$ network, (b) $C-R//C$ network, (c) $R-R//C$. The map colour indicates the probability value.

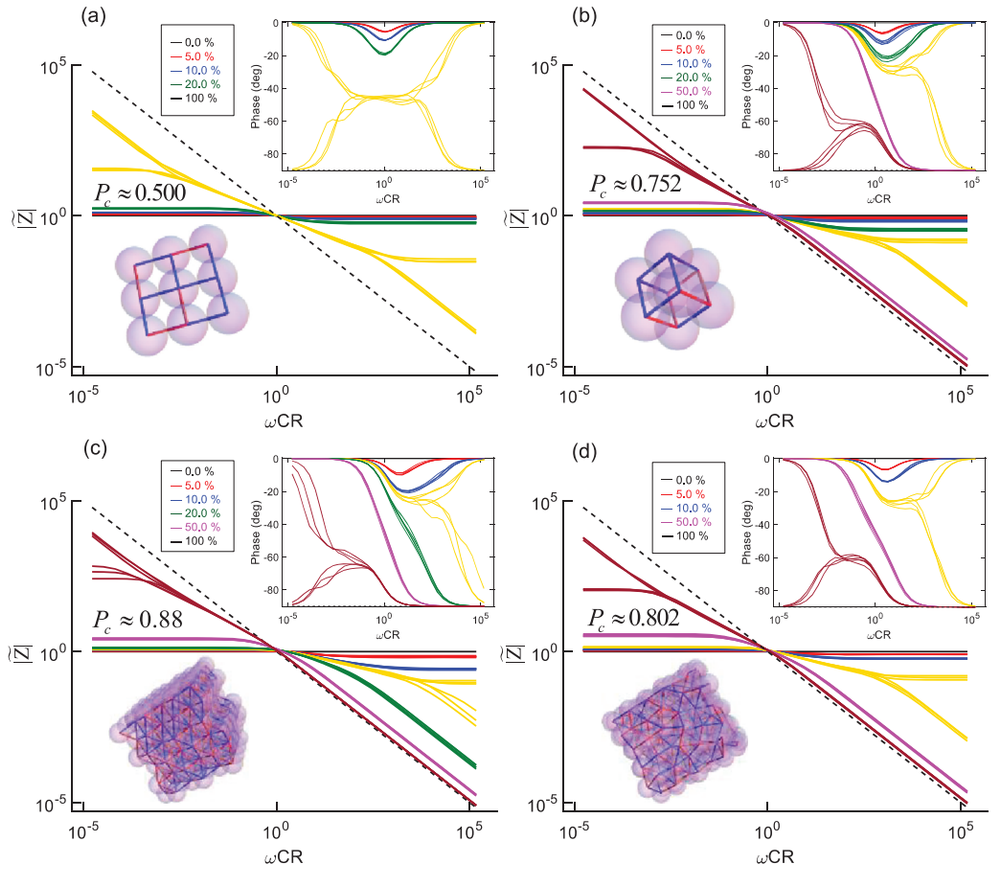

Fig. 2. Normalised impedance module as a function of frequency for various RC networks: (a) 2D lattice square network with 40×40 spheres; (b) 3D SC packing with $12 \times 12 \times 12$ spheres; (c) 3D FCC packing with 1688 spheres; (d) random packing containing 1600 spheres with a packing factor of 0.62 ± 0.006. The insert to the top-right shows the impedance phase versus frequency. The insert to the left-bottom shows the packing structure, with the electrical contacts indicated by pillars (red for R and blue for C). Ten realizations have been shown in each individual scenario. Realizations of various capacitor proportions, P_C, are shown in lines of different colours. Percolation thresholds, P_S, at low frequency are calculated using Monte Carlo method and provided in the figure. The AC responses with P_C being the calculated percolation threshold are shown in dark red curves. The AC responses with P_R being the percolation threshold are shown in yellow curves. The AC responses of networks with only R and C elements are presented by solid and dashed black lines, respectively.

module, $|\tilde{Z}|$ on normalised frequency, $\tilde{\omega}$, based on 2D square, SC (simple cubic), random and FCC (face-cantered cubic) packing structures. Each contact is assigned to be either R or C, which has the identical value throughout the network. The normalisation of $|Z|$ and ω is calculated by

$$|\tilde{Z}| = |Z|/Z_R, \quad \tilde{\omega} = \omega CR \tag{5}$$

where Z_R is the resistance for a given network structure with all components being resistors, e.g., $P_C = 0$. Features including the resistive plateau, NCL state, emergent power-law segment and the intersection point can be found in Figure 2, demonstrating the intrinsic electrical characteristics of AC responses.

The onset and termination of the emergent power-law segment were found to be corresponding to the peaks of spectra of admittance, Z'', and electrical module, M'', respectively, as is typically shown in Figure 3. Here, Z' and Z'' are the real and imaginary part of Z, respectively, and M'' is calculated by $M'' = \omega Z'$. Peaks observed in Z'' and M'' spectra indicate the occurrence of two relaxation processes that are associated with the path alternation of current percolation as a result of competition between resistive and capacitive paths. As frequency increases, the transport of current is consequently accomplished by the paths fabricated by capacitors due to the significantly larger conductance then that of the resistors at the given frequency. For frequencies between peaks of Z'' and M'' spectra, the capacitors and resistors exhibiting comparative conductance cooperatively regulate the current path, giving rise to emergent power-law scaling regions. Here the range between peaks of Z'' and M'' spectra is defined as the length of power-law segment.

4. EXPERIMENTAL OBSERVATIONS

In order to examine the proposed analytical and numerical approaches, and also to reveal the origins of observed

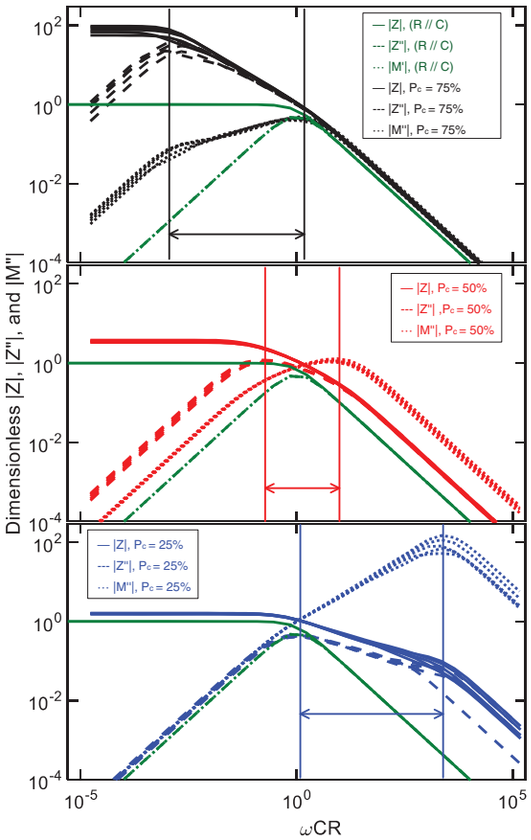

Fig. 3. Spans of power law scaling segment in $|Z|$ spectra (solid lines), between the peaks of $|Z''|$ spectra (dashed lines) and $|M''|$ spectra (dotted lines). Networks is realized based on random packings of 1000 spheres with a packing factor of 0.63 containing R and C components. Five typical realizations are presented for each individual scenario for P_c equalling 75%, 50%, and 25%, corresponding to curves in black, red and blue, respectively. Electrical responses of the equivalent network containing a resistor and capacitor in parallel are shown in green as references.

emergent power-law scaling, we measured AC spectra of conductive granular mixtures. Stainless steel (AISI 304, with precision grade G200) spheres and glass beads of 2 mm were randomly packed in a nonconductive cylinder (Al_2O_3) with circular steel plates as top and bottom electrodes. Impedance spectra were measured using an impedance analyser (Agilent 4294A) from 40 Hz to 10 MHz, and plotted as a function of frequency ω as shown in Figure 4(a). We performed isobaric measurements for packings containing only steel spheres under various normal compression (from 2.16 to 3.40 kPa) and mixtures under a load of 7.76 kPa. All mixtures have the same number of steel grains (around 21,600) but varying number of glass beads. Within the applied pressure range, all obtained impedance values are considerably larger than the total resistance (<10 mΩ) of the measurement system excluding the packed bed under testing. In order to minimize current-induced local welding, we applied an AC signal with a peak-to-peak value of 200 mV, through which linear ohmic behaviour can be observed in current–voltage responses for the considered loading range.[3, 46, 47] Controlled measurements were performed to exclude parasitic resonance signals from cabling and connections, using measured Nyquist plots.[48] Similar to Eq. (5) the measured impedance module was normalised by δR_{dc} where δ indicates the ratio of steel number with respect to the total grain number and R_{dc} is the measured resistance at the frequency of 40 Hz. The frequency was normalised by the recognised frequency, ω_Z^* at the peak of $|Z''|$ spectrum. As is shown in Figure 4(b), the impedance spectra measured for packings of only steel spheres under various compression collapse onto a single master curve, while AC responses for mixtures demonstrate different lengths of power-law segments between resistive plateau and the NCL segment. Noted that, for packings with only steel spheres, peaks of $|M''|$ spectra could not be extracted within the considered frequency range as is shown in the bottom subfigure of Figure 4(a). Therefore, the corresponding length of power-law segment can be not be properly calculated.

The length of the power-law segment of experimentally observed AC responses was extracted from simulation results using numerical approach described previously. Here steel spheres were considered to be randomly distributed in the packing, establishing a RC network from the steel-to-steel contact fabric. A few necessary assumptions have been made for simplification as suggested in Ref. [12]: (a) Either C or $R//C$ components are randomly assigned to each individual contact. This assumption is further supported by results shown in Figure 1 as we obtained both resistive plateau and NCL at 40 Hz for cases of $P_m = 0.3$ in experiments; (b) All R and C element have identical resistance and capacitance values, respectively; (c) The overall capacitor proportion is assumed to be 70% based on the power law slope observed in experiments. With the same assumptions listed-above, the length of the power-law segment was also calculated based on percolation theory, as is presented in Section 2. For each P_m, the value of percolation threshold is calculated based on RC network established from the prescribed packing structures realised by DEM. The percolation-based analytical approach is able to efficiently compute the AC response for various types of RC network, but the detailed information near the intersections of segments would be missed. As is shown in Figure 4(c), both analytical and numerical frameworks agree well with experimental results, demonstrating the role of percolation behaviour in dominating central power law segments, thus the whole AC response spectra. It is noticeable that all the three assumptions are strongly associated with the inter-particle properties, especially for $P_c = 0.7$ which is a pivotal input parameter for both circuit simulation and theoretical approaches.

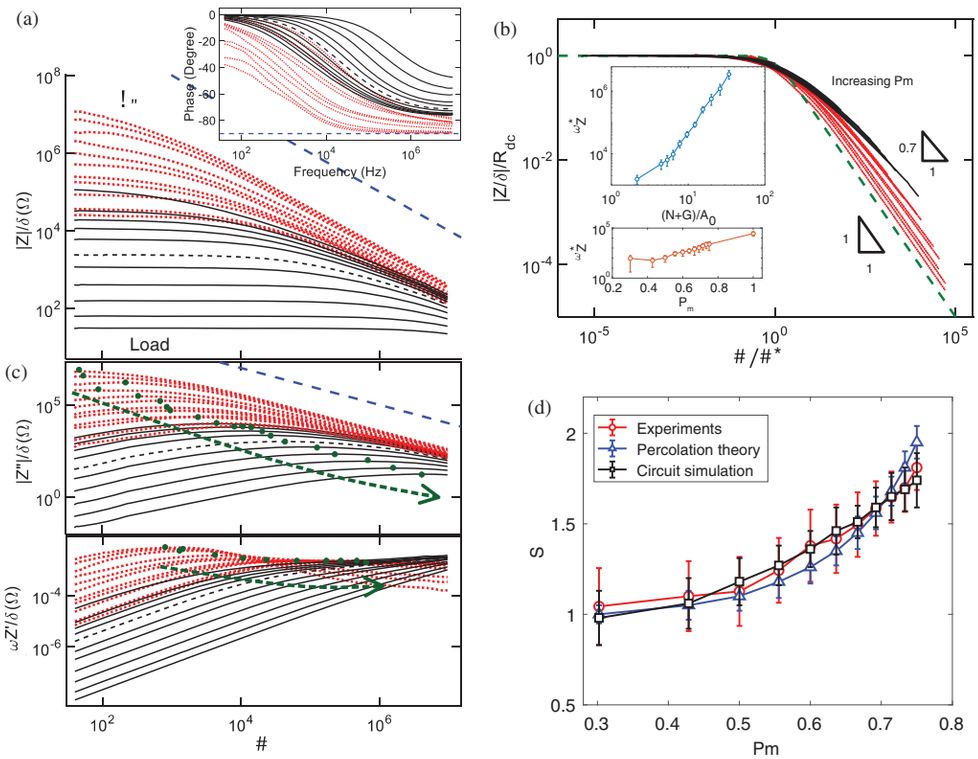

Fig. 4. (a) Typical spectra of $|Z|$, $|Z''|$, and $|M''|$ on frequency for packings with steel spheres under various loads and granular mixtures. The insert shows the impedance phase versus frequency. Blue dashed line indicates AC responses of packings with only glass beads. The red arrow indicates the increasing trend of P_m and the black arrow indicates the increasing trend of applied load. In the spectra of $|Z''|$, and $|M''|$, peaks were marked by green dots; (b) scaling of the normalised $|Z|$ on normalised ω. The top insert presents the dependence of the characteristic ω_Z^* recognized at peaks of $|Z''|$ spectra on normalized normal compression, $(N+G)/A_0$, where N is the applied normal compression, G is the half of the gravitational force of the packing, A_0 is the cross-section area of the granular packing. For mixtures with varying of steel sphere fraction, P_m, the characteristic ω_Z^* recognised at peaks of $|Z''|$ spectra are shown in the bottom insert; (c) comparison of the length of power-law segment obtained from experiments, percolation theory and DEM simulations. The error bars for experimental results are calculated based on four groups of tests. The results from numerical simulations and percolation theory were averaged over ten realisations.

5. CONCLUSION

We investigated AC responses of conductive granular mixtures based on percolation theory and circuit simulation focusing on the spans of emergent universal power-law scaling. We further validated both analytical and numerical results with experimental observations of AC responses of conductive granular mixtures with various proportion of conductive grains. The considered granular packings were treated as RC networks based on contact fabrics, which were reproduced by DEM to provide network configuration for analytical and numerical approaches. The present results demonstrate that by considering the topological configurations of conductive granular systems along with the physical characteristics of intergranular contacts, AC responses in conductive granular materials can be meaningfully captured. We have shown how the power law scaling and transition from resistive plateau to NCL emerge as a consequence of percolation, which in turn is governed by network characteristics. The proposed analytical and numerical frameworks are helpful for transport analyses of conductive granular mixtures, connecting the microscopic features to the effective properties, and, furthermore, provide guidelines in developing testing techniques for granular energy systems.

References and Notes

1. R. Sachser, F. Porrati, C. H. Schwalb, and M. Huth; Universal conductance correction in a tunable strongly coupled nanogranular metal; *Physical Review Letters* 107, 206803 (**2011**).
2. H. Bakkali, M. Dominguez, X. Batlle, and A. Labarta; Universality of the electrical transport in granular metals; *Scientific Reports* 6, 29676 (**2016**).
3. M. Creyssels, E. Falcon, and B. Castaing; Scaling of ac electrical conductivity of powders under compression; *Physical Review B* 77, 075135 (**2008**).
4. J. C. Dyre and T. B. Schrøder; Universality of ac conduction in disordered solids; *Reviews of Modern Physics* 72, 873 (**2000**).
5. W. Li and R. W. Schwartz; Ac conductivity relaxation processes in $CaCu_3Ti_4O_{12}$ ceramics: Grain boundary and domain boundary effects; *Applied Physics Letters* 89, 242906 (**2006**).
6. D. P. Almond and C. Bowen; Anomalous power law dispersions in ac conductivity and permittivity shown to be characteristics of microstructural electrical networks; *Physical Review Letters* 92, 157601 (**2004**).

7. J. C. Dyre, P. Maass, B. Roling, and D. L. Sidebottom; Fundamental questions relating to ion conduction in disordered solids; *Reports on Progress in Physics* 72, 046501 **(2009)**.
8. T. B. Schrøder and J. C. Dyre; Ac hopping conduction at extreme disorder takes place on the percolating cluster; *Physical Review Letters* 101, 025901 **(2008)**.
9. S. Elliott; Ac conduction in amorphous chalcogenide and pnictide semiconductors; *Advances in Physics* 36, 135 **(1987)**.
10. V. Etacheri, R. Marom, R. Elazari, G. Salitra, and D. Aurbach; Challenges in the development of advanced Li-ion batteries: A review; *Energy and Environmental Science* 4, 3243 **(2011)**.
11. D. Sidebottom; Colloquium: Understanding ion motion in disordered solids from impedance spectroscopy scaling; *Reviews of Modern Physics* 81, 999 **(2009)**.
12. C. Zhai, Y. Gan, D. Hanaor, and G. Proust; Stress-dependent electrical transport and its universal scaling in granular materials; *Extreme Mechanics Letters* 22, 83 **(2018)**.
13. D. P. Almond, C. Bowen, and D. Rees; Composite dielectrics and conductors: Simulation, characterization and design; *Journal of Physics D: Applied Physics* 39, 1295 **(2006)**.
14. D. P. Almond, C. J. Budd, and N. J. McCullen; Emergent behaviour in large electrical networks; Approximation Algorithms for Complex Systems, Springer, Berlin, Heidelberg **(2011)**, pp. 3–26.
15. D. Almond, C. Budd, M. Freitag, G. Hunt, N. McCullen, and N. Smith; The origin of power-law emergent scaling in large binary networks; *Physica A: Statistical Mechanics and Its Applications* 392, 1004 **(2013)**.
16. C. Zhai, D. Hanaor, G. Proust, L. Brassart, and Y. Gan; Interfacial electro-mechanical behaviour at rough surfaces; *Extreme Mechanics Letters* 9, 422 **(2016)**.
17. C. Zhai, D. Hanaor, and Y. Gan; Universality of the emergent scaling in finite random binary percolation networks; *Plos One* 12, e0172298 **(2017)**.
18. D. Chen, Z. Lin, H. Zhu, and R. J. Kee; Percolation theory to predict effective properties of solid oxide fuel-cell composite electrodes; *Journal of Power Sources* 191, 240 **(2009)**.
19. B. Völker and R. M. McMeeking; Impact of particle size ratio and volume fraction on effective material parameters and performance in solid oxide fuel cell electrodes; *Journal of Power Sources* 215, 199 **(2012)**.
20. J. Ott, B. Völker, Y. Gan, R. M. McMeeking, and M. Kamlah; A micromechanical model for effective conductivity in granular electrode structures; *Acta Mechanica Sinica* 29, 682 **(2013)**.
21. N. J. Mccullen, D. P. Almond, C. J. Budd, and G. W. Hunt; The robustness of the emergent scaling property of random *RC* network models of complex materials; *Journal of Physics D: Applied Physics* 42, 064001 **(2009)**.
22. K. Murphy, G. Hunt, and D. P. Almond; Evidence of emergent scaling in mechanical systems; *Philosophical Magazine* 86, 3325 **(2006)**.
23. K. Bourbatache, M. Guessasma, E. Bellenger, V. Bourny, and A. Tekaya; Discrete modelling of electrical transfer in multi-contact systems; *Granular Matter* 14, 1 **(2012)**.
24. D. Almond and B. Vainas; The dielectric properties of random *R-C* networks as an explanation of the universal' power law dielectric response of solids; *Journal of Physics: Condensed Matter* 11, 9081 **(1999)**.
25. R. Marom, S. F. Amalraj, N. Leifer, D. Jacob, and D. Aurbach; A review of advanced and practical lithium battery materials; *Journal of Materials Chemistry* 21, 9938 **(2011)**.
26. W. Bauer, D. Nötzel, V. Wenzel, and H. Nirschl; Influence of dry mixing and distribution of conductive additives in cathodes for lithium ion batteries; *Journal of Power Sources* 288, 359 **(2015)**.
27. J. R. Macdonald and E. Barsoukov; Impedance spectroscopy: Theory, experiment, and applications; *History* 1, 1 **(2005)**.
28. D. Abraham, J. Heaton, S.-H. Kang, D. Dees, and A. Jansen; Investigating the low-temperature impedance increase of lithium-ion cells; *J. Electrochem. Soc.* 155, A41 **(2008)**.
29. S. Srivastav, M. J. Lacey, and D. Brandell; State-of-charge indication in Li-ion batteries by simulated impedance spectroscopy; *Journal of Applied Electrochemistry* 47, 229 **(2017)**.
30. U. S. Kim, C. B. Shin, and C.-S. Kim; Effect of electrode configuration on the thermal behavior of a lithium-polymer battery; *Journal of Power Sources* 180, 909 **(2008)**.
31. U. S. Kim, C. B. Shin, and C.-S. Kim; Modeling for the scale-up of a lithium-ion polymer battery; *Journal of Power Sources* 189, 841 **(2009)**.
32. D. V. Do, C. Forgez, K. E. K. Benkara, and G. Friedrich; Impedance observer for a Li-ion battery using Kalman filter; *IEEE Transactions on Vehicular Technology* 58, 3930 **(2009)**.
33. M. Yilmaz and P. T. Krein; Review of battery charger topologies, charging power levels, and infrastructure for plug-in electric and hybrid vehicles; *IEEE Transactions on Power Electronics* 28, 2151 **(2013)**.
34. M. S. Islam and C. A. Fisher; Lithium and sodium battery cathode materials: Computational insights into voltage, diffusion and nanostructural properties; *Chemical Society Reviews* 43, 185 **(2014)**.
35. J. Xu, C. C. Mi, B. Cao, and J. Cao; A new method to estimate the state of charge of lithium-ion batteries based on the battery impedance model; *Journal of Power Sources* 233, 277 **(2013)**.
36. P. Costamagna, P. Costa, and V. Antonucci; Micro-modelling of solid oxide fuel cell electrodes; *Electrochimica Acta* 43, 375 **(1998)**.
37. C. Zhai, D. Hanaor, G. Proust, and Y. Gan; Stress-dependent electrical contact resistance at fractal rough surfaces; *Journal of Engineering Mechanics* 143, B4015001 **(2015)**.
38. C. Zhai, D. Hanaor, G. Proust, and Y. Gan; Stress-dependent frequency response of conductive granular materials; *62th Holm Conference on Electrical Contacts*, IEEE **(2016)**, pp. 9–16.
39. C. Zhai, Y. Gan, D. Hanaor, G. Proust, and D. Retraint; The role of surface structure in normal contact stiffness; *Experimental Mechanics* 56, 359 **(2016)**.
40. R. L. Jackson, E. R. Crandall, and M. J. Bozack; Rough surface electrical contact resistance considering scale dependent properties and quantum effects; *Journal of Applied Physics* 117, 195101 **(2015)**.
41. P. G. Slade; Electrical Contacts: Principles and Applications; CRC Press, London, UK **(2013)**.
42. A. Aharony and D. Stauffer; Introduction to Percolation Theory; Taylor & Francis **(2003)**.
43. M. Sahimi; Applications of Percolation Theory; CRC Press, Boca Raton, Florida **(1994)**.
44. J. K. Ott; Modeling the Microstructural and Micromechanical Influence on Effective Properties of Granular Electrode Structures with regard to Solid Oxide Fuel Cells and Lithium Ion Batteries, Karlsruhe Institute of Technology **(2015)**.
45. Y. Gan and M. Kamlah; Discrete element modelling of pebble beds: With application to uniaxial compression tests of ceramic breeder pebble beds; *Journal of the Mechanics and Physics of Solids* 58, 129 **(2010)**.
46. C. Zhai, D. Hanaor, G. Proust, L. Brassart, and Y. Gan; Interfacial electro-mechanical behaviour at rough surfaces; *Extreme Mechanics Letters* 9, 422 **(2016)**.
47. A. Basu, G. Adams, and N. McGruer; A review of micro-contact physics, materials, and failure mechanisms in direct-contact RF MEMS switches; *Journal of Micromechanics and Microengineering* 26, 104004 **(2016)**.
48. B. Roling; What do electrical conductivity and electrical modulus spectra tell us about the mechanisms of ion transport processes in melts, glasses, and crystals? *Journal of Non-Crystalline Solids* 244, 34 **(1999)**.